NANO LETTERS
Cite This: Nano Lett. XXXX, XXX, XXX−XXX
Letter
pubs.acs.org/NanoLett

Nanoparticle Size Influences Antigen Retention and Presentation in Lymph Node Follicles for Humoral Immunity

Yi-Nan Zhang,[†,‡] James Lazarovits,[†,‡,¶] Wilson Poon,[†,‡,¶] Ben Ouyang,[†,‡,§,¶] Luan N. M. Nguyen,[†,‡] Benjamin R. Kingston,[†,‡] and Warren C. W. Chan*[,†,‡,∥,⊥,#]

[†]Institute of Biomaterials & Biomedical Engineering, University of Toronto, Toronto, Ontario M5S 3G9, Canada
[‡]Terrence Donnelly Centre for Cellular & Biomolecular Research, University of Toronto, Toronto, Ontario M5S 3E1, Canada
[§]MD/PhD Program, Faculty of Medicine, University of Toronto, Toronto, Ontario M5S 1A8, Canada
[∥]Department of Chemical Engineering & Applied Chemistry, University of Toronto, Toronto, Ontario M5S 3E5, Canada
[⊥]Department of Materials Science & Engineering, University of Toronto, Toronto, Ontario M5S 1A1, Canada
[#]Department of Chemistry, University of Toronto, Toronto, Ontario M5S 3H6, Canada

Supporting Information

ABSTRACT: Lymph node follicles capture and retain antigens to induce germinal centers and long-lived humoral immunity. However, control over antigen retention has been limited. Here we discovered that antigen conjugated to nanoparticle carriers of different sizes impacts the intralymph node transport and specific cell interaction. We found that follicular dendritic cell (FDC) networks determine the intralymph node follicle fate of these nanoparticles by clearing smaller ones (5−15 nm) within 48 h and retaining larger ones (50−100 nm) for over 5 weeks. The 50−100 nm-sized nanoparticles had 175-fold more delivery of antigen at the FDC dendrites, 5-fold enhanced humoral immune responses of germinal center B cell formation, and 5-fold more antigen-specific antibody production over 5−15 nm nanoparticles. Our results show that we can tune humoral immunity by simply manipulating the carrier size design to produce effectiveness of vaccines.

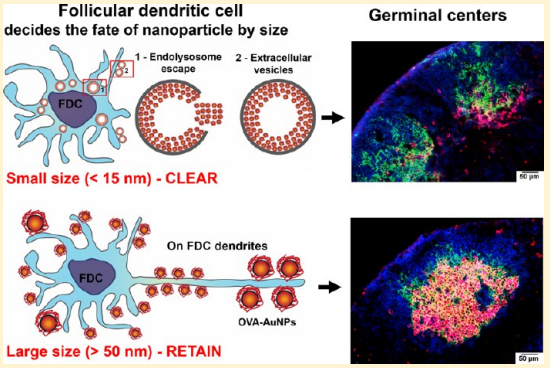

KEYWORDS: *Nanoparticle, lymph node, antigen retention and presentation, follicular dendritic cells, germinal centers, complement*

Efficient vaccination requires long-lived germinal center reactions to drive antibody-mediated humoral immunity.[1−4] Antigens must be retained and presented to B cells in lymph node follicles to generate an effective humoral immune response.[5−8] A proposed strategy is to use engineered nanoparticles to deliver antigens into follicles.[5,9−13] Tuning the size of the nanoparticle alters its transport to the lymph node follicle.[6,14,15] Interestingly, 5 nm nanoparticles such as toll-like receptor agonists flow directly to lymph node follicles, whereas 100 nm nanoparticles such as viruses require cell-mediated transport into follicles.[11,16−24] Although it is generally known that lymph node physiology mediates nanoparticle transport to follicles in a size-dependent matter, it is unclear how different sizes of nanoparticles interact with cells inside follicles to influence: (1) follicular retention, (2) antigen presentation, (3) germinal center formation, and (4) antigen-specific antibody production. A better understanding of the interaction of nanoparticle design with the lymph node system can guide the rational/optimal engineering of nanoparticles to drive germinal center reactions that generate antibody-mediated humoral immunity for efficient vaccination.

We first studied the relationship between nanoparticle size and follicle retention in the lymph node. We synthesized a model nanoparticle vaccine composed of different sizes of spherical gold nanoparticles (AuNPs) conjugated to ovalbumin (OVA) antigen. The full characterization of the nanoparticle physicochemical properties is described in Figure S1 and Table S1. We chose AuNPs because of the following: (1) they can be easily synthesized with broad and precise sizes in the 2 to 100 nm size range; (2) they are nondegradable, which allows long-term tracking at the organ and cellular levels; and (3) they can be coated with multiple molecules, which enables them to be used as an adjuvant and delivery vehicle for antigen peptides or proteins.[25−29] These sub-100 nm nanoparticles should transport from the injection site to sentinel lymph nodes through the lymphatics[15,30−32] (Figure 1A). We expect that the size of the nanoparticles mediates their kinetics, binding, and other interactions with cells and biological structures in the lymph nodes. Once nanoparticles enter the afferent lymphatic vessel of a lymph node, they need to pass a two-layer filter system,[33,34] subcapsular sinus macrophages and lymphatic

Received: July 11, 2019
Revised: September 3, 2019
Published: September 11, 2019

DOI: 10.1021/acs.nanolett.9b02834
Nano Lett. XXXX, XXX, XXX−XXX

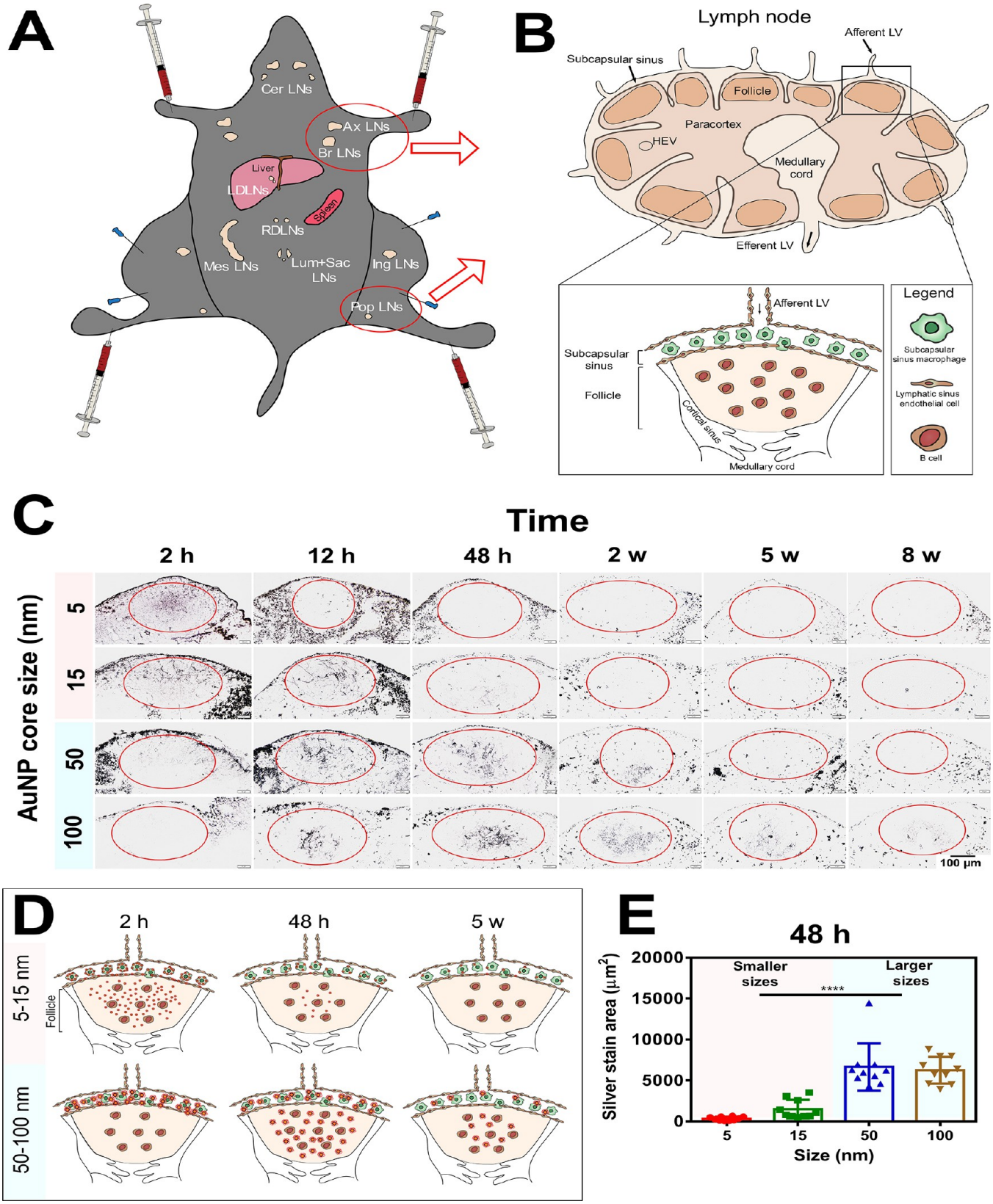

Figure 1. Lymph node follicles clear smaller nanoparticles and retain larger ones. (A) Schematic of lymph node distribution. OVA-AuNPs were injected into C57BL/6 mice through intradermal footpad administration. Axillary (Ax), brachial (Br), and popliteal (Pop) lymph nodes are defined as sentinel lymph nodes. (B) Schematics of a lymph node that are made of subcapsular sinus, follicle, paracortex, and medullary cord areas. Lymph nodes are considered as a two-layer size-selective filter system that is composed of subcapsular sinus macrophages and lymphatic sinus endothelial cells before entering B cell follicles. (C) Histological images of different OVA-AuNP sizes cleared or retained in lymph node follicles after 2 h to 8 weeks post intradermal footpad injection into C57BL/6 mice (n = 4 mice/group). Lymph node follicles of sentinel lymph nodes were collected. Data collected from 10 lymph node follicles (n = 4). The injection dose was normalized on the basis of the same OVA antigen amount (10 μg) for

DOI: 10.1021/acs.nanolett.9b02834
Nano Lett. XXXX, XXX, XXX−XXX

Figure 1. continued

each size. (D) Schematic of the size-dependent OVA-AuNP transport kinetics. The 5−15 nm OVA-AuNPs appeared in the follicles within 2 h but are cleared in the next 48 h. The 50−100 nm OVA-AuNPs accumulated at the subcapsular sinus at 2 h. They had delayed follicle accumulation and were retained for over 5 weeks. (E) Quantification of different sizes of OVA-AuNP accumulation in follicles at 48 h postinjection. Data collected from 10 lymph node follicles (n = 4). Graphs represent mean ± SD; ****P < 0.0001. All P values are from one-way ANOVA followed by Tukey's multiple comparisons test.

sinus endothelial cells, before entering the lymph node follicles and interacting with B cells (Figure 1B). We administered our model OVA-AuNP vaccine through intradermal footpad injections into C57BL/6 mice (Figure 1A). The injection dose was normalized on the basis of the same total amount of OVA (10 μg) for each size (Figure S1 and S2). The normalizing of dosing in our study enables us to test the impact of nanoparticle size on their lymph node interaction. We sacrificed the mice after different injection times (from 2 h to 8 weeks) and collected the axillary, brachial, and popliteal as sentinel lymph nodes for histological analysis (Figure 1B). We stained the sample with silver to enhance the AuNP signal on the tissue. We observed a clear difference between different nanoparticle sizes and their intralymph node transport and retention in follicles (Figure 1C, S3). The smaller OVA-AuNPs (5−15 nm) appeared in the follicles within 2 h but were cleared in the next 48 h. The larger OVA-AuNPs (50−100 nm) accumulated in subcapsular sinus at 2 h. They required a longer time to accumulate in follicles and were retained for over 5 weeks (Figure 1D). The 50−100 nm OVA-AuNPs showed greater retention than the 5−15 nm ones after 48 h of injection. Notably, 50 nm OVA-AuNPs show 19-fold and 4-fold greater amounts of nanoparticles accumulated in lymph node follicles than 5 and 15 nm OVA-AuNPs at 48 h (Figure 1E). These results confirmed a clear relationship between nanoparticle size and lymph node follicle retention.

We determined the lymph node cells involved with the retention of nanoparticles. We know from previous studies that follicular dendritic cells (FDCs) are resident stromal cells that form networks located in the follicle centers and are the only known cell type that acquire and retain naïve antigens for months.[35−39] FDC networks reserve these naïve antigens and present them to B cells for B cell activation and generation of germinal center reactions.[5,8,14,40−42,] Therefore, FDCs were a logical candidate to mediate both the sequestration and retention of OVA-AuNPs inside lymph node follicles. The mice were sacrificed at the peak OVA-AuNP accumulation times in lymph node follicles (2 h for 5 and 15 nm OVA-AuNPs, and 48 h for 50 and 100 nm OVA-AuNPs). To preserve the antigens on the cell membrane, isolated fresh lymph nodes were directly placed into frozen solution in a plastic cryomold and frozen with liquid nitrogen. Tissue sections (8 μm) were cut and placed on charged slides. Tissue sections were stained using silver enhancement kits to enhance gold nanoparticle signal and antibody immunostaining for FDCs and other cell types. We found the AuNP signal (silver staining) colocalized with the networks of CD21$^+$ FDCs in the 5−15 nm (Figure 2A and Figure S4A) and the 50−100 nm OVA-AuNP (Figure 2B and Figure S4B) tissue samples. CD21$^+$ FDCs are highlighted by the green color staining in Figure 2A,B and Figure S4. To verify the histology stain for FDCs, we co-stained this cell type using another FDC-M1 antibody (Figure 2C). FDC-M1 (red color) and CD21 (green color) stains are colocalized on FDCs. We also show that T cells (CD3$^+$), tingible body macrophages (CD68$^+$), and

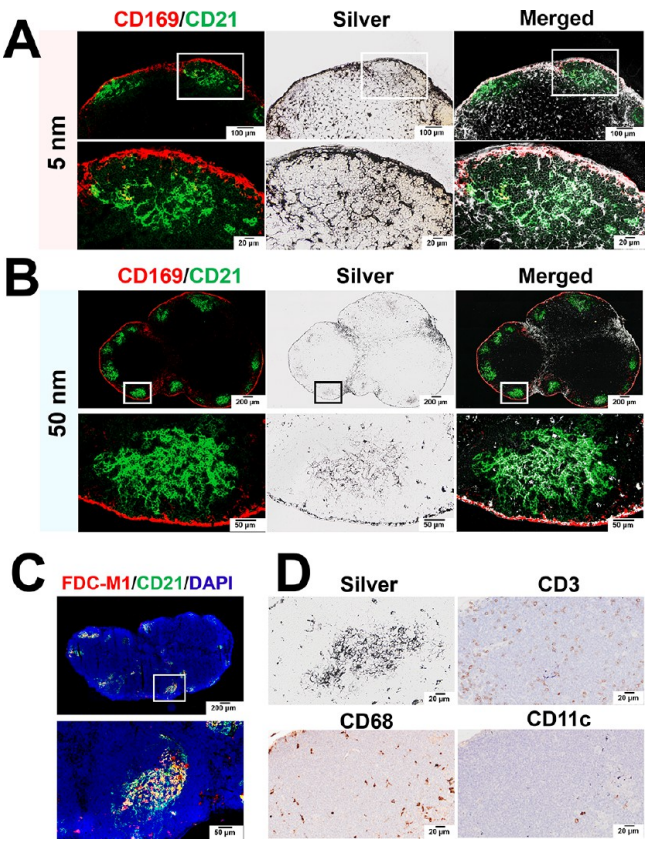

Figure 2. FDC networks are involved in nanoparticle sequestration in lymph node follicles. Histology of (A) 5 nm and (B) 50 nm OVA-AuNP sequestration in lymph node follicles associated with FDC networks at 2 and 48 h post intradermal footpad injection. Gold nanoparticle signals colocalized in the area of FDC networks (CD21 green; CD169 red; Silver black). (C) Validation of antibody staining for FDCs in lymph node follicles. FDC-M1 (red) and CD21 (green) stains colocalized on FDCs. (D) OVA-AuNP signals are not colocalized with T cells (CD3) (brown), tingible body macrophages (CD68) (brown), and dendritic cells (CD11c) (brown), indicating that they are not majorly involved in sequestration of OVA-AuNPs in lymph node follicles.

dendritic cells (CD11c$^+$) are not the major cell types involved in sequestration of the OVA-AuNPs (Figure 2D). This is because these stained immune cells (brown colors) were not corresponding to the area of OVA-AuNP signals (silver staining). We confirmed this conclusion using 3D images of lymph nodes after CLARITY processing.[43,44] The results show that FDCs formed network clusters (green color) and OVA-AuNPs (red color) were colocalized in these FDC networks (Figure S5). Our results confirmed the role of FDCs in mediating the retention of nanoparticles inside of the lymph node follicle.

We further analyzed whether the nanoparticles are inside the FDCs or on their dendrites. The mice were sacrificed after the peak OVA-AuNP accumulation times in lymph node follicles.

DOI: 10.1021/acs.nanolett.9b02834
Nano Lett. XXXX, XXX, XXX−XXX

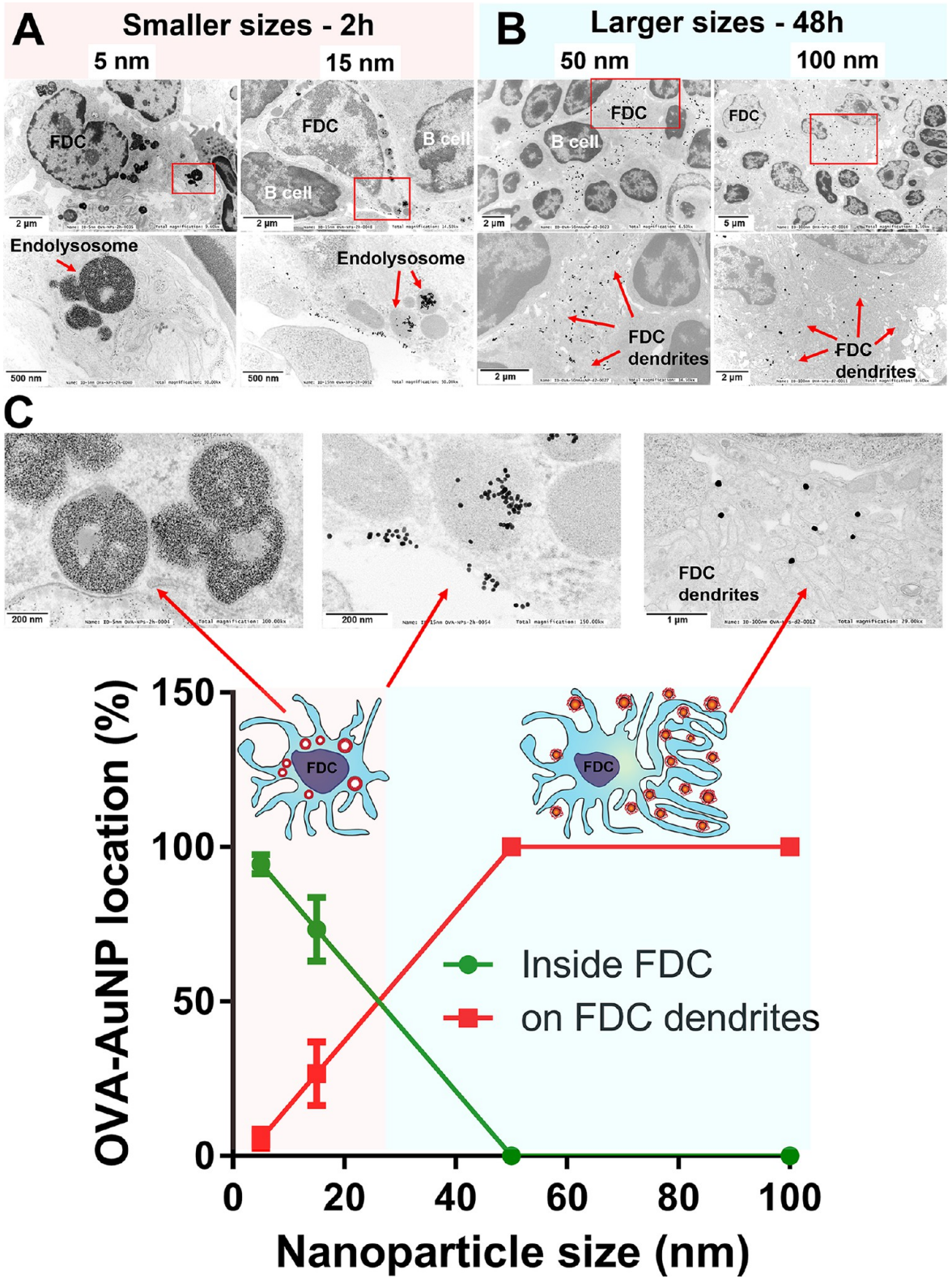

Figure 3. FDCs internalize smaller nanoparticles and align larger nanoparticles on their surfaces and dendrites. (A,B) Representative TEM images of nanoparticle location associated with FDCs in a size-dependent manner. TEM study was performed at different times of postintradermal footpad injection (the 5−15 OVA-AuNPs at 2 h; the 50−100 nm OVA-AuNPs at 48 h). (A) The 5 nm OVA-AuNPs are preferentially internalized by FDCs (red arrows point to endolysosomes), and (B) the 50−100 nm OVA-AuNPs are preferred to be aligned on FDC surfaces and dendrites (red arrows point to FDC dendrites). (C) Quantification of nanoparticle location either inside the FDC or on FDC dendrites. TEM images and schematics of 5 nm OVA-AuNPs internalized by FDCs while 50−100 nm OVA-AuNPs retained on FDC surface or dendrites. The 15 nm OVA-AuNPs can be both inside the FDC or on FDC surface. Data collected from 3 sentinel lymph nodes for each nanoparticle size (n = 3−4 mice/group).

DOI: 10.1021/acs.nanolett.9b02834
Nano Lett. XXXX, XXX, XXX−XXX

The sentinel lymph nodes were collected and directly fixed with 4% formaldehyde and 0.5% glutaraldehyde in PBS. The fixed samples were mounted and sectioned, then placed on copper grids. The sample sections were subjected to negative staining with 2% uranyl acetate. The morphology of FDCs and nanoparticle localization of lymph node sections were imaged using transmission electron microscopy (TEM) at 200 kV. TEM analysis showed that the residence of OVA-AuNPs inside or out of the FDCs is size-dependent (Figure 3A,B). The 5 nm OVA-AuNPs are internalized in the endolysosome-like structures of FDCs, while the 50−100 OVA-AuNPs are aligned on the FDC surfaces or dendrites (Figure 3C). The 15 nm OVA-AuNPs can reside inside the FDC or on the FDC surface. While the 5 nm OVA-AuNPs were trapped in endolysosome-like structures (Figure 3A), interestingly, we observed instances where the endolysosomal membrane were disrupted and 5 nm OVA-AuNPs were found in the cytoplasm (Figure 4A). This is shown by the green arrow. We also found extracellular vesicles containing 5 nm OVA-AuNPs (red circles) attached to the FDC surface (Figure 4A). These results suggest that 5 nm OVA-AuNPs can be cleared by FDCs through endolysosomal escape or extracellular vesicles within 48 h. These cleared 5 nm OVA-AuNPs by FDCs were further eliminated from lymph node follicles (Figure 1C). In contrast, the 50−100 nm OVA-AuNPs remained on the surface of the FDCs, with most of them residing on the dendrites (Figure 4B). They were retained on the dendrites for a few weeks. We conclude that the size of the nanoparticles determines when they are taken up by the FDCs or reside on the cell surface and dendrites.

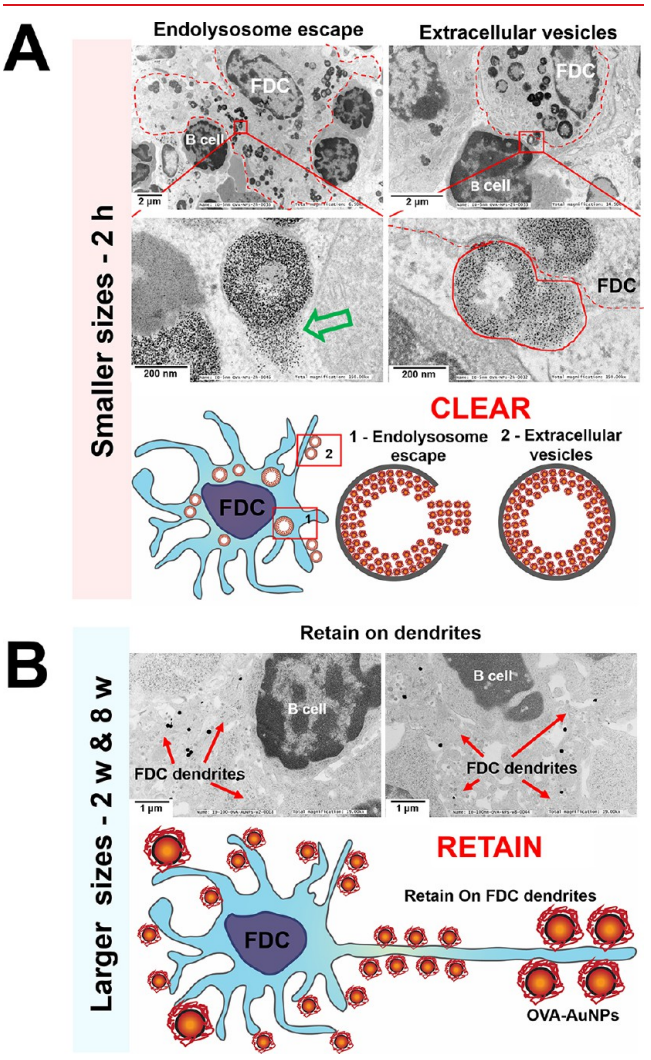

Figure 4. FDCs clear smaller nanoparticles by endolysosomal escape and extracellular vesicles and retain larger ones on their dendrites. (A) TEM images and schematics of 5 nm OVA-AuNPs cleared through endolysosomal escape or exosomes. (B) TEM images and schematics of 100 nm OVA-AuNPs retained on FDC dendrites over a few weeks. Data collected from 3 sentinel lymph nodes for each nanoparticle size (n = 3−4 mice/group).

Next, we tested how nanoparticle size mediates antigen presentation on the FDC dendrites. We administered different sizes of OVA-AuNPs through intradermal footpad injections into C57BL/6 mice and sacrificed the mice at 48 h. The sentinel lymph nodes were isolated and fixed. We sectioned the lymph node tissues and placed them on copper grids for TEM study. TEM revealed that B cells were surrounded by FDC dendrites containing the OVA-AuNPs (Figure 5A,B). The FDC dendrites deposited with OVA-AuNPs grip B cells that facilitates the interaction of conjugated-antigen and B cell receptors. There were significantly more 50 and 100 nm OVA-AuNPs on FDC dendrites than 5 nm OVA-AuNPs at 48 h (Figure 5C−E). In addition, 100 nm AuNPs can conjugate 317-fold and 100-fold more OVA than the 5 and 15 nm AuNPs, respectively (Figure S2). This leads to 175-fold more OVA bound to the FDC dendrites by the 100 nm AuNPs in comparison to the 15 nm AuNPs (Figure 5F). This result suggests 50−100 nm OVA-AuNPs can present more antigen on FDC dendrites to B cells.

This allowed us to test if the 50−100 nm OVA-AuNPs would induce more humoral immune responses over the smaller 5−15 nm OVA-AuNPs. We immunized the mice using different sizes of OVA-AuNP vaccine and sacrificed the mice at 5 weeks. The isolated lymph nodes were frozen in a plastic cryomold. The lymph node tissue sections were cut and stained with anti-OVA antibody for OVA and other antibodies for immunostaining. Our result shows that 100 nm AuNPs were still colocalized with OVA in the follicles, confirming that the OVA remained conjugated to the AuNPs after 5 weeks of injection (Figure 6A). We first observed germinal center generation as a measurement of humoral immune response. We performed histological analysis for germinal centers using an anti-GL7 stain. We observed that 100 nm OVA-AuNPs can induce germinal centers (red color) that attach FDC networks (green color), and 100 nm OVA-AuNPs are still colocalized with FDC networks after 5 weeks of immunization (Figure 6B). We performed histology for all sizes. The 50 and 100 nm OVA-AuNPs could induce germinal centers (red color), whereas the 5 nm OVA-AuNPs failed to generate robust germinal center reactions (Figure 6C,D). We further quantified the total number of $GL7^{+}B220^{+}$ germinal center B cells by disaggregation of the lymph node into single cells for flow cytometry (Figure 6E,F and Figure S6). We found that the 100 nm OVA-AuNPs generated 5-fold more germinal center B cells than 5 nm OVA-AuNPs (Figure 6F). These findings confirm that the retained 50 and 100 nm OVA-AuNPs on FDC dendrites can induce greater stimulation of germinal center reactions and proliferation of germinal center B cells. Next, we quantified the amount of OVA-specific antibody in the sera using enzyme-linked immunosorbent assay (ELISA) to determine if the 100 nm OVA-AuNPs elicited greater antigen-specific antibody production. We determined that 5-

DOI: 10.1021/acs.nanolett.9b02834
Nano Lett. XXXX, XXX, XXX−XXX

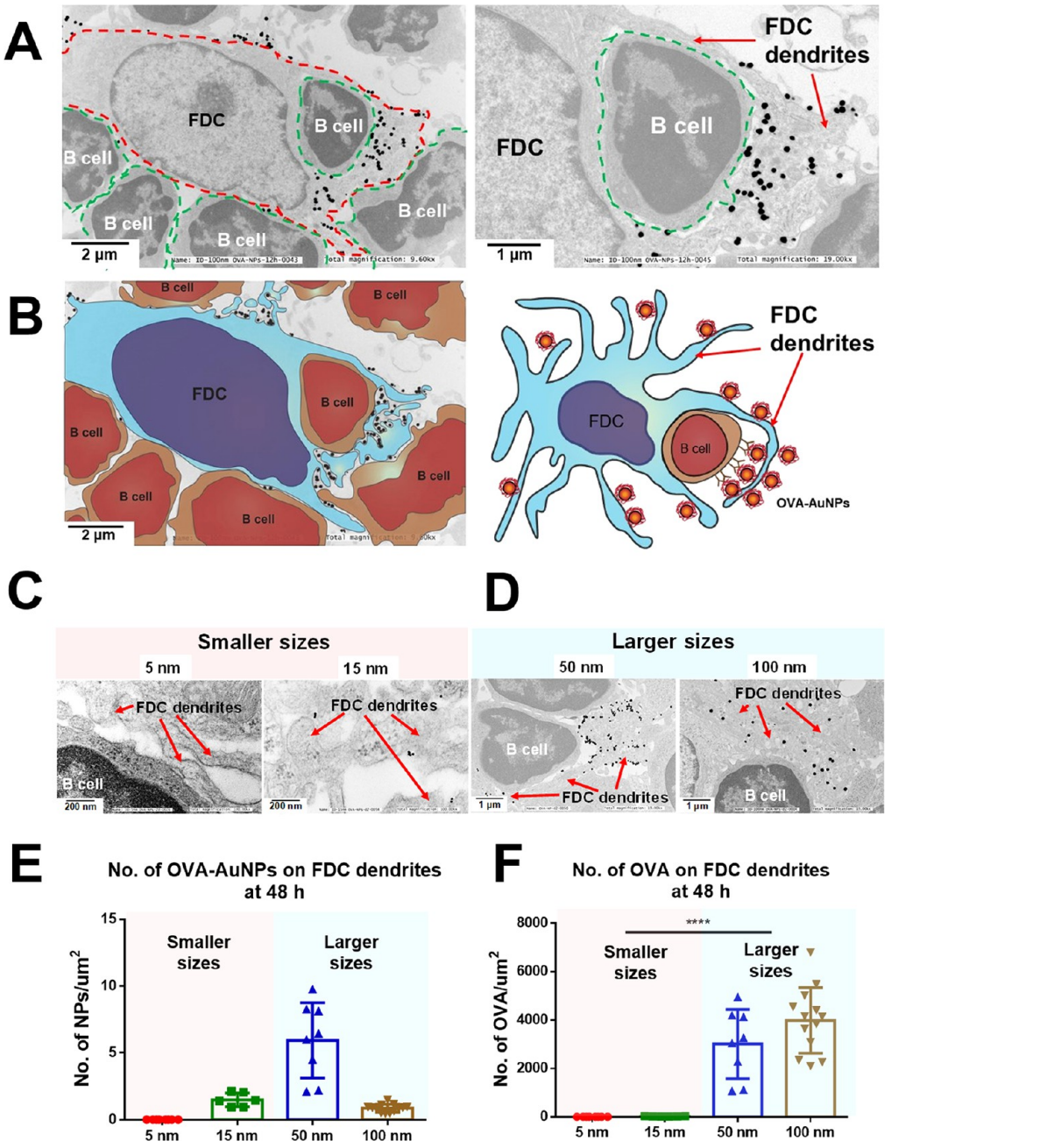

Figure 5. 50−100 nm sized nanoparticles have greater deposition on FDC dendrites leading to more conjugated antigens presentation on FDC to stimulate B cells. (A) Representative TEM images of FDC dendrites surrounding B cells containing OVA-AuNPs (red arrows point to FDC dendrites). (B) Schematics of (A) showing OVA-AuNPs are deposited on FDC surfaces and dendrites. FDC dendrites surrounding B cells with OVA-AuNPs that facilitates the interaction of conjugated-antigen and B cell receptors. (C,D) TEM images of different sizes of OVA-AuNPs depositing and presenting conjugated-antigen on FDC dendrites at 48 h post intradermal footpad injection. Red arrows point to the FDC dendrites. Quantifying (E) numbers of OVA-AuNPs and (F) numbers of conjugated OVA on FDC dendrites at 48 h. Data collected from 3 sentinel lymph nodes for each nanoparticle size (n = 3−4 mice/group). Data shown as mean ± SD; ****P < 0.0001. All P values are from one-way ANOVA followed by Tukey's multiple comparisons tests.

fold more OVA-specific antibody was produced in response to 100 nm OVA-AuNPs than the 5 nm OVA-AuNPs (Figure 6G). We conclude that the conjugation of OVA to 50−100 nm nanoparticles can induce greater humoral immune responses than 5−15 nm nanoparticles because more conjugated antigens are bound and presented on FDC dendrites to stimulate B cells.

While OVA is involved in generating an antigen-specific immune response, we were curious to know why the nanoparticles are bound to receptors on the FDCs. Our recent study showed that nanoparticles opsonize serum proteins when they are administered into the animal.[45] Previously, we used mass spectrometry to identify the adsorbed proteins. Thus, we have a list of candidates that can be tested to identify the specific proteins that may be responsible for the receptor−ligand interaction. We hypothesize that complement C3 was opsonized on the nanoparticle surface and this ligand is responsible for its interaction with the

DOI: 10.1021/acs.nanolett.9b02834
Nano Lett. XXXX, XXX, XXX−XXX

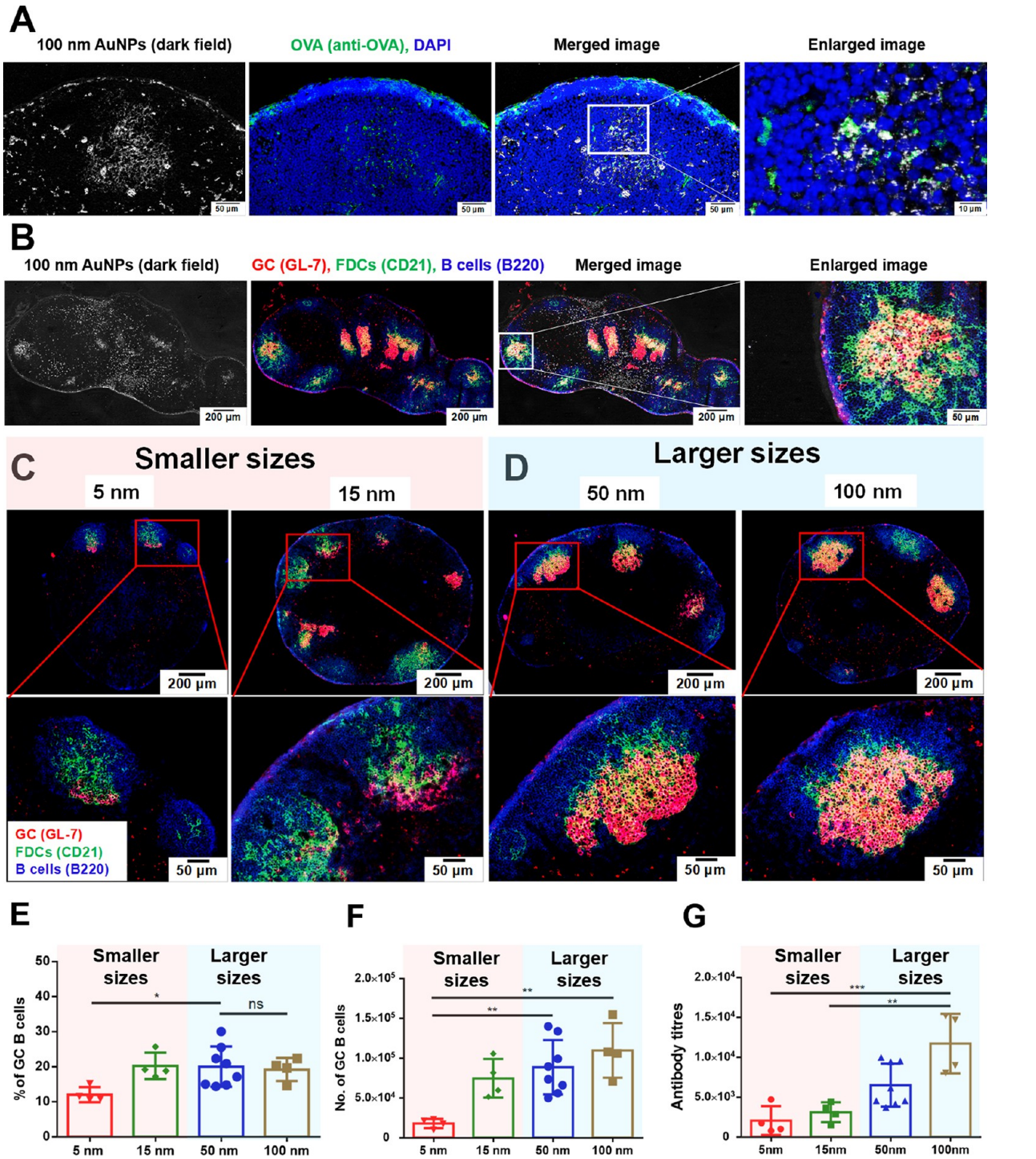

Figure 6. 50−100 nm sized nanoparticle vaccines induce greater humoral immune responses. (A) Colocalization of 100 nm AuNPs with OVA antigen in follicles after 5 weeks of injection. Anti-OVA stain colocalized with AuNP signal generated by dark field microscopy, indicating that the OVA remained conjugated to the AuNPs. (B) Colocalization of 100 nm OVA-AuNPs with FDCs in germinal centers after 5 weeks of immunization. FDC colocalized with AuNP signal generated by dark field microscopy. Assessment of (C and D) germinal center formation (GL7 red; CD21 green; B220 blue), (E) percentage of germinal center B cells ($GL7^+B220^+$), (F) numbers of germinal center B cells ($GL7^+B220^+$), and (G) antigen-specific antibody production in sera after intradermal footpad injection with different sizes of OVA-AuNP vaccine at 5 weeks (n = 4−8 mice/group). The injection dose is normalized on the basis of the same amount of OVA antigen (10 μg) for each nanoparticle size. Data shown as mean ± SD; $^{**}P < 0.01$; $^{***}P < 0.001$; $^{****}P < 0.0001$. All P values are from one-way ANOVA followed by Tukey's multiple comparisons tests.

FDC through complement receptor 2 (CR2) (Figure S7). This hypothesis is built on previous findings that virus and bacteria require opsonization by complement C3.[6,14,35,46,47] We performed experiments with C3 and CR2knockout mice, and we used CD19 knockout mice as a negative control. It has been shown previously that inhibition of CD19 receptors disables B cell stimulation and germinal center formation.[48,49] Here, we expected that even though OVA-AuNPs were retained and presented on FDC dendrites, OVA-AuNPs should not induce humoral immune responses in CD19

DOI: 10.1021/acs.nanolett.9b02834
Nano Lett. XXXX, XXX, XXX−XXX

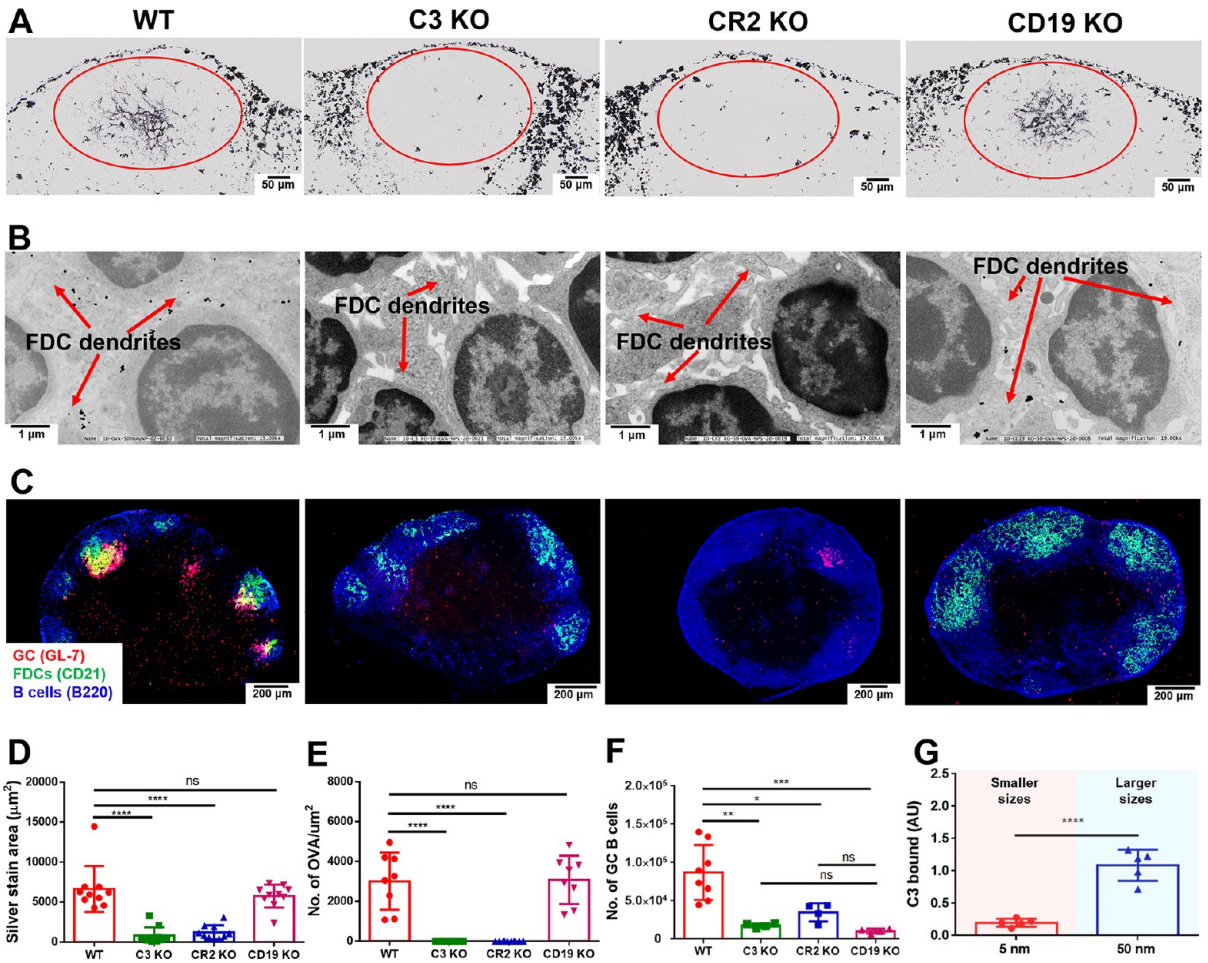

Figure 7. 50−100 nm sized nanoparticle vaccines induce high amounts of complement opsonization resulting in enhanced nanoparticle retention, antigen presentation on FDC dendrites, and germinal center reactions. (A−F) Study of nanoparticle retention, antigen presentation and germinal center reactions in wild type and C3, CR2 and CD19 receptor knockout mice after intradermal footpad injection with 50 nm OVA-AuNP vaccines. (A and D) Histology of OVA-AuNP sequestration in lymph node follicles at 48 h (n = 4 mice/group in C57BL/6 background). (B and E) Representative TEM images of AuNP conjugated antigen presentation on FDC dendrites at 48 h. Data collected from 3 sentinel lymph nodes for each condition (n = 3−4 mice/group). Assessment of (C) germinal center formation (B220 blue; CD21 green; GL7 red) and (F) numbers of germinal center B cells ($GL7^+B220^+$) after intradermal footpad injection with 50 nm OVA-AuNP vaccine at 5 weeks (n = 4−8 mice/group). (G) Quantification of the complement C3 adsorbed on OVA-AuNP surfaces using ELISA (AU stands for arbitrary units, n = 5). Graphs represent mean ± SD; $^*P < 0.05$; $^{**}P < 0.01$; $^{***}P < 0.001$; $^{****}P < 0.0001$. All P values are from one-way ANOVA followed by Tukey's multiple comparisons tests or an unpaired t test.

knockout mice. We injected the C3, CR2, and CD19 receptor knockout mice with 50 nm OVA-AuNP vaccines and sacrificed the mice after 48 h and 5 weeks, respectively (Figure 7A−F). We determined a loss of complement (either C3 or CR2) prevented OVA-AuNP retention in follicles (Figure 7A,D) and OVA-AuNP presentation on FDC dendrites (Figure 7B,E) at 48 h. We determine that a loss of C3 protein failed to induce germinal centers at 5 weeks (Figure 7C). Both complement knockout mice (C3 protein and CR2) produced significantly lower numbers of germinal center B cells than wild types and showed no significant difference compared with CD19 knockout mice at 5 weeks (Figure 7F). These results show that the C3−CR2 ligand−receptor pair assists the retention and presentation of OVA-AuNPs on the FDCs, leading to germinal center reactions. We then tested for OVA-specific antibody production using ELISA. Surprisingly, we found loss of complements did not limit OVA-specific antibody production (Figure S8). The mechanism is unknown and will be explored later. To test if nanoparticle opsonization by C3 is based on nanoparticle size, we designed a modified ELISA experiment where different sizes of OVA-AuNPs were precoated onto plates and incubated with wild-type mice sera. Our results show that 50 nm OVA-AuNPs have greater C3 deposition than 5 nm ones *in vitro* (Figure S9). To verify that OVA-AuNPs follow the same principle *in vivo*, we performed the same ELISA experiment on 5 and 50 nm OVA-AuNPs isolated from lymph nodes *in vivo* at 1 and 6 h postinjection. Similarly, we found more C3 adsorbed onto 50 nm OVA-AuNPs than 5 nm ones (Figure 7G). These results suggest that larger OVA-AuNPs are opsonized by complements more than smaller ones, leading to enhanced nanoparticle retention, antigen presentation on FDC dendrites, and more robust germinal center reactions.

In this study, we discovered that the physiology of the lymph node determines the kinetics and cellular interaction of the nanoparticles. Sub-100 nm nanoparticles can transport through the lymph node. However, the intralymph node fate is determined by the size. The 5−15 nm nanoparticles can

DOI: 10.1021/acs.nanolett.9b02834
Nano Lett. XXXX, XXX, XXX−XXX

enter the FDCs, while the 50−100 nm remained on the surface. The binding of the nanoparticles to the dendrites were greater with the 50−100 nm due to the greater adsorption of complement C3. Our study reveals the mechanism of how lymph node follicles process different nanoparticle sizes. This provides us with fundamental knowledge on how biological selection of antigens occurs and functions. Our report provides results for gold nanoparticles with OVA only. The role of organic or inorganic synthetic nanoparticles with other antigens on how to shape the acquired immune responses should be fully assessed in the future. The results of these findings will guide the rational design of antigen-conjugated synthetic nanoparticles in mediating FDC interaction for more effective vaccine development.

■ ASSOCIATED CONTENT

Supporting Information

The Supporting Information is available free of charge on the ACS Publications website at DOI: 10.1021/acs.nanolett.9b02834.

Materials and methods, nanoparticle vaccine characterization, physicochemical properties of nanoparticle vaccines, quantification of numbers of OVA protein on AuNPs using bicinchoninic acid (BCA) assay, quantification of silver stained area in histology images of different sizes of OVA-AuNP retention in lymph node follicles over 8 week, and other data as mentioned in the text (PDF)

■ AUTHOR INFORMATION

Corresponding Author

*E-mail: warren.chan@utoronto.ca.

ORCID

Warren C. W. Chan: 0000-0001-5435-4785

Author Contributions

¶J.L., W.P., and B.O. contributed equally to this work. Y.-N.Z. and W.C.W.C. conceptualized the project. Y.-N.Z., J.L., and L.N.M.N. designed, synthesized, and characterized nanoparticles and nanoparticle vaccines. Y.-N.Z., J.L., W.P., B.O., and B.R.K. designed, performed, and analyzed experiments. Y.-N.Z. and W.C.W.C. wrote the initial manuscript draft. All authors contributed to review and editing of the manuscript.

Notes

The authors declare no competing financial interest.

■ ACKNOWLEDGMENTS

We thank K.M. Tsoi, A.J. Tavares, Y. Zhang, S. Sindhwani, A.M. Syed, and F. Song from our lab for fruitful discussions. Y.-N.Z. acknowledges Prof. Michael Carroll at Harvard Medical School for valuable discussion and comments on 2D and 3D images of nanoparticle interaction with follicular dendritic cells and complement knockout mice studies. Y.-N.Z. acknowledges Z. Hao at The Donnelly Centre for Cellular and Biomolecular Research of University of Toronto for valuable suggestion and discussion on humoral immune function tests. We thank D. Holmyard and A. Darbandi at The Hospital for Sick Children Nanoscale Biomedical Imaging Facility for TEM sample preparation and their expertise in TEM operation. We thank M. Ganguly, L. Morikawa, S. Newbigging, V. Bradaschia, Q. Xu, and A. Ramirez at the Toronto Centre for Phenogenomics for their expertise in histology and immunostaining. We thank D. White and J. Warzyszynska at Faculty of Medicine Flow Cytometry Facility of Univeristy of Toronto and O. Rojas at the Department of Immunology Faculty of Medicine of University of Toronto for their expertise in flow cytometry. This study was supported by Canadian Cancer Society Research Institute, Canadian Institutes of Health Research (CIHR) Grant MOP-130143, Natural Sciences and Engineering Research Council of Canada (NSERC) Grant 2015-06397, and a Collaborative Health Research Project (CHRP-493619-16). Y.-N.Z. thanks NSERC, OGS, Wildcat Foundation, and Paul and Sally Wang for provision of fellowships and graduate scholarships. J.L. thanks NSERC fellowships. W.P. thanks CIHR, OGS, Barbara and Frank Milligan, and Cecil Yip for provision of fellowships and graduate scholarships. B.O. thanks the Vanier Canada Graduate Scholarship, CIHR and the McLaughlin Centre for MD/PhD studentships, and the Donnelly Centre for graduate fellowships. B.R.K. thanks NSERC, the Wildcat Foundation, the Donnelly Centre and the Royal Bank of Canada (RBC) Graduate fellowship for student scholarships and funding. Last but not least, Y.-N.Z. thanks his family for their continuous support during this project, his grandma F.P. Zhu, his mother M. Guan, mother-in-law H.Z. Zhang, and especially his wife B. Gao.

■ REFERENCES

(1) Allen, C. D. C.; Okada, T.; Cyster, J. G. *Immunity* **2007**, *27* (2), 190−202.

(2) Mesin, L.; Ersching, J.; Victora, G. D. *Immunity* **2016**, *45* (3), 471−482.

(3) Victora, G. D.; Nussenzweig, M. C. *Annu. Rev. Immunol.* **2012**, *30*, 429−457.

(4) Kasturi, S. P.; Skountzou, I.; Albrecht, R. A.; Koutsonanos, D.; Hua, T.; Nakaya, H. I.; Ravindran, R.; Stewart, S.; Alam, M.; Kwissa, M.; Villinger, F.; Murthy, N.; Steel, J.; Jacob, J.; Hogan, R. J.; García-Sastre, A.; Compans, R.; Pulendran, B. *Nature* **2011**, *470* (7335), 543−547.

(5) Rappuoli, R. *Sci. Transl. Med.* **2018**, *10* (456), eaat4615.

(6) Cyster, J. G. *Nat. Immunol.* **2010**, *11* (11), 989−996.

(7) McHeyzer-Williams, M.; Okitsu, S.; Wang, N.; McHeyzer-Williams, L. *Nat. Rev. Immunol.* **2012**, *12* (1), 24−34.

(8) Cyster, J. G.; Allen, C. D. C. *Cell* **2019**, *177* (3), 524−540.

(9) Sun, X.; Stefanetti, G.; Berti, F.; Kasper, D. L. *Proc. Natl. Acad. Sci. U.S.A.* **2019**, *116* (1), 193−198.

(10) Tokatlian, T.; Read, B. J.; Jones, C. A.; Kulp, D. W.; Menis, S.; Chang, J. Y. H.; Steichen, J. M.; Kumari, S.; Allen, J. D.; Dane, E. L.; Liguori, A.; Sangesland, M.; Lingwood, D.; Crispin, M.; Schief, W. R.; Irvine, D. J. *Science* **2019**, *363* (6427), 649−654.

(11) Mueller, S. N.; Tian, S.; DeSimone, J. M. *Mol. Pharmaceutics* **2015**, *12* (5), 1356−1365.

(12) Wilson, J. T. *Science* **2019**, *363* (6427), 584−585.

(13) Marcandalli, J.; Fiala, B.; Ols, S.; Perotti, M.; de van der Schueren, W.; Snijder, J.; Hodge, E.; Benhaim, M.; Ravichandran, R.; Carter, L.; Sheffler, W.; Brunner, L.; Lawrenz, M.; Dubois, P.; Lanzavecchia, A.; Sallusto, F.; Lee, K. K.; Veesler, D.; Correnti, C. E.; Stewart, L. J.; Baker, D.; Loré, K.; Perez, L.; King, N. P. *Cell* **2019**, *176* (6), 1420−1431.e17.

(14) Batista, F. D.; Harwood, N. E. *Nat. Rev. Immunol.* **2009**, *9* (1), 15−27.

(15) Bachmann, M. F.; Jennings, G. T. *Nat. Rev. Immunol.* **2010**, *10* (11), 787−796.

(16) Roozendaal, R.; Mempel, T. R.; Pitcher, L. A.; Gonzalez, S. F.; Verschoor, A.; Mebius, R. E.; von Andrian, U. H.; Carroll, M. C. *Immunity* **2009**, *30* (2), 264−276.

(17) Phan, T. G.; Green, J. A.; Gray, E. E.; Xu, Y.; Cyster, J. G. *Nat. Immunol.* **2009**, *10* (7), 786−793.

DOI: 10.1021/acs.nanolett.9b02834
Nano Lett. XXXX, XXX, XXX−XXX

(18) Phan, T. G.; Grigorova, I.; Okada, T.; Cyster, J. G. *Nat. Immunol.* **2007**, *8* (9), 992−1000.
(19) Junt, T.; Moseman, E. A.; Iannacone, M.; Massberg, S.; Lang, P. A.; Boes, M.; Fink, K.; Henrickson, S. E.; Shayakhmetov, D. M.; Di Paolo, N. C.; van Rooijen, N.; Mempel, T. R.; Whelan, S. P.; von Andrian, U. H. *Nature* **2007**, *450* (7166), 110−114.
(20) Gonzalez, S. F.; Lukacs-Kornek, V.; Kuligowski, M. P.; Pitcher, L. A.; Degn, S. E.; Kim, Y.-A.; Cloninger, M. J.; Martinez-Pomares, L.; Gordon, S.; Turley, S. J.; Carroll, M. C. *Nat. Immunol.* **2010**, *11* (5), 427−434.
(21) Gonzalez, S. F.; Degn, S. E.; Pitcher, L. A.; Woodruff, M.; Heesters, B. A.; Carroll, M. C. *Annu. Rev. Immunol.* **2011**, *29*, 215−233.
(22) Kuka, M.; Iannacone, M. *Nat. Rev. Immunol.* **2018**, *18* (4), 255−265.
(23) Heinen, E.; Braun, M.; Coulie, P. G.; van Snick, J.; Moeremans, M.; Cormann, N.; Kinet-Denoël, C.; Simar, L. J. *Eur. J. Immunol.* **1986**, *16* (2), 167−172.
(24) Carrasco, Y. R.; Batista, F. D. *Immunity* **2007**, *27* (1), 160−171.
(25) Lee, I.-H.; Kwon, H.-K.; An, S.; Kim, D.; Kim, S.; Yu, M. K.; Lee, J.-H.; Lee, T.-S.; Im, S.-H.; Jon, S. *Angew. Chem., Int. Ed.* **2012**, *51* (35), 8800−8805.
(26) Niikura, K.; Matsunaga, T.; Suzuki, T.; Kobayashi, S.; Yamaguchi, H.; Orba, Y.; Kawaguchi, A.; Hasegawa, H.; Kajino, K.; Ninomiya, T.; Ijiro, K.; Sawa, H. *ACS Nano* **2013**, *7* (5), 3926−3938.
(27) Wei, M.; Chen, N.; Li, J.; Yin, M.; Liang, L.; He, Y.; Song, H.; Fan, C.; Huang, Q. *Angew. Chem., Int. Ed.* **2012**, *51* (5), 1202−1206.
(28) Lazarovits, J.; Chen, Y. Y.; Song, F.; Ngo, W.; Tavares, A. J.; Zhang, Y.-N.; Audet, J.; Tang, B.; Lin, Q.; Tleugabulova, M. C.; Wilhelm, S.; Krieger, J.; Mallevaey, T.; Chan, W. C. W. *Nano Lett.* **2019**, *19* (1), 116−123.
(29) Li, X.; Wang, X.; Ito, A. *Chem. Soc. Rev.* **2018**, *47* (13), 4954−4980.
(30) Swartz, M. A.; Hirosue, S.; Hubbell, J. A. *Sci. Transl. Med.* **2012**, *4* (148), 148rv9.
(31) Maisel, K.; Sasso, M. S.; Potin, L.; Swartz, M. A. *Adv. Drug Delivery Rev.* **2017**, *114*, 43−59.
(32) Irvine, D. J.; Swartz, M. A.; Szeto, G. L. *Nat. Mater.* **2013**, *12* (11), 978−990.
(33) Hons, M.; Sixt, M. *Nat. Immunol.* **2015**, *16* (4), 338−340.
(34) Rantakari, P.; Auvinen, K.; Jäppinen, N.; Kapraali, M.; Valtonen, J.; Karikoski, M.; Gerke, H.; Iftakhar-E-Khuda, I.; Keuschnigg, J.; Umemoto, E.; Tohya, K.; Miyasaka, M.; Elima, K.; Jalkanen, S.; Salmi, M. *Nat. Immunol.* **2015**, *16* (4), 386−396.
(35) Heesters, B. A.; Myers, R. C.; Carroll, M. C. *Nat. Rev. Immunol.* **2014**, *14* (7), 495−504.
(36) Kosco-Vilbois, M. H. *Nat. Rev. Immunol.* **2003**, *3* (9), 764−769.
(37) Szakal, A. K.; Kosco, M. H.; Tew, J. G. *Annu. Rev. Immunol.* **1989**, *7*, 91−109.
(38) Allen, C. D. C.; Cyster, J. G. *Semin. Immunol.* **2008**, *20* (1), 14−25.
(39) Rodda, L. B.; Lu, E.; Bennett, M. L.; Sokol, C. L.; Wang, X.; Luther, S. A.; Barres, B. A.; Luster, A. D.; Ye, C. J.; Cyster, J. G. *Immunity* **2018**, *48* (5), 1014−1028.e6.
(40) Wang, X.; Cho, B.; Suzuki, K.; Xu, Y.; Green, J. A.; An, J.; Cyster, J. G. *J. Exp. Med.* **2011**, *208* (12), 2497−2510.
(41) Tew, J. G.; Wu, J.; Fakher, M.; Szakal, A. K.; Qin, D. *Trends Immunol.* **2001**, *22* (7), 361−367.
(42) Tew, J. G.; Wu, J.; Qin, D.; Helm, S.; Burton, G. F.; Szakal, A. K. *Immunological Reviews* **1997**, *156*, 39−52.
(43) Sindhwani, S.; Syed, A. M.; Wilhelm, S.; Glancy, D. R.; Chen, Y. Y.; Dobosz, M.; Chan, W. C. W. *ACS Nano* **2016**, *10* (5), 5468−5478.
(44) Syed, A. M.; Sindhwani, S.; Wilhelm, S.; Kingston, B. R.; Lee, D. S. W.; Gommerman, J. L.; Chan, W. C. W. *J. Am. Chem. Soc.* **2017**, *139* (29), 9961−9971.
(45) Lazarovits, J.; Sindhwani, S.; Tavares, A. J.; Zhang, Y.; Song, F.; Audet, J.; Krieger, J. R.; Syed, A. M.; Stordy, B.; Chan, W. C. W. *ACS Nano* **2019**, *13* (7), 8023−8034.
(46) Carroll, M. C. *Annu. Rev. Immunol.* **1998**, *16*, 545−568.
(47) Dempsey, P. W.; Allison, M. E. D.; Akkaraju, S.; Goodnow, C. C.; Fearon, D. T. *Science* **1996**, *271* (5247), 348−350.
(48) Rickert, R. C.; Rajewsky, K.; Roes, J. *Nature* **1995**, *376* (376), 352−355.
(49) Carroll, M. C. *Semin. Immunol.* **1998**, *10* (4), 279−286.

NOTE ADDED AFTER ASAP PUBLICATION

This paper was published ASAP on September 17, 2019 before all the corrections were received. The paper was revised and the new version was reposted on September 18, 2019.

DOI: 10.1021/acs.nanolett.9b02834
Nano Lett. XXXX, XXX, XXX−XXX